J Electroceram (2008) 21:837–841
DOI 10.1007/s10832-007-9310-4

Neodymium substituted $Bi_4Ti_3O_{12}$ nanostructures through self-assembly

J. Ma · X. M. Lu · Y. Kan · J. Gu · J. S. Zhu

Published online: 27 August 2007

Abstract For the sake of fabricating the ultrahigh density ultralarge scale integration (ULSI) memory chips, the ferroelectric nanostructures fabricated through self-assembly are studied. In this paper, we synthesized the neodymium substituted $Bi_4Ti_3O_{12}$ nanostructures on Pt/Ti/SiO_2/Si substrates. The method we used here was spin coating precursors with a series of different concentrations on the substrates and then annealing at 750 °C in the oxygen atmosphere to get the self-patterning nanoparticles. In order to avoid the influence of the Pt/Ti/SiO_2/Si substrates to the largest extent, the substrates were annealed first for different time in oxygen atmosphere to select appropriate conditions. Scanning probe microscope, and X-ray diffraction were used to detect the morphology and the crystalline structure of the nanoparticles respectively. The well-separated $Bi_{3.15}Nd_{0.85}Ti_3O_{12}$ particles have a typical lateral size about 100–150 nm and height about 20–25 nm. XRD reveals pyrochlore phase in the low concentration samples. The lower the precursor's concentration, the higher the excess of Bi element is needed to form the pure perovskite nanoparticles.

Keywords Nanostructure · Nd-substituted $Bi_4Ti_3O_{12}$ · Self-assembly

PACS 81.16.Dn · 77.80.-e · 81.07.-b

J. Ma · X. M. Lu · Y. Kan · J. Gu · J. S. Zhu (✉)
National laboratory of Solid State Microstructures,
Department of Physics, Nanjing University,
Nanjing 210093, China
e-mail: jszhu@nju.edu.cn

1 Introduction

Bismuth-layered perovskite ferroelectric materials, especially the lanthanide and neodymium substituted $Bi_4Ti_3O_{12}$, have attracted much attention due to their applications in nonvolatile random access memory devices because of their rather good ferroelectric properties [1–4]. Comparing with $Bi_{3.25}La_{0.75}Ti_3O_{12}$, the $Bi_{3.15}Nd_{0.85}Ti_3O_{12}$ thin films have nearly the same polarization values but better fatigue properties in the low frequency. In order to get the ferroelectric memories in gigabit densities, a memory unit should be limited to a hundred nanometers in the thickness or less. Comparing with the submicron lithography, the ferroelectric nanostructures growth through self-assembly are studied. M. Alexe, and J. F. Scott had done a series of important works in this area. Their main works are self-assembly fabricating the ferroelectric epitaxial nanocrystals and self-partterning nano-electrodes on the epitaxial ferroelectric thin films [5–8]. We tried to self-assemble the neodymium substituted $Bi_4Ti_3O_{12}$ nanostructures on Pt/Ti/SiO_2/Si substrates. The method we used was spin coating precursors on the substrates and then annealing in the oxygen atmosphere to get the self-patterning nanoparticles. The effect of the concentration and the amount of Bi excess on the microstructure was investigated.

2 Experiment

Pt has been the most heavily studied and successfully used noble metal for the bottom electrodes. In order to avoid the influence of the Pt/Ti/SiO_2/Si substrate to the largest extent, the substrates with 200 nm thick Pt and 20 nm thick Ti layers were annealed first for different time in oxygen atmosphere to select appropriate conditions. $Bi_{3.15}Nd_{0.85-}$

Ti_3O_{12} (BNT) nano particles were deposited on Pt (111)/Ti/SiO_2/Si substrates by metal-organic decomposition (MOD) method using Bismuth nitrate, Neodymium nitrate, and Butyl titanate as the precursors. Bismuth nitrate normally with 10% stoichiometric excess and neodymium nitrate were first mixed in an appropriate ratio, then dissolved in glacial acetic acid. After an equimolar amount of Butyl titanate added into the solution, ethyleneglycnl monomethyl ether was used to achieve a concentration of 0.1 mol/l. Finally a small amount of acetylacetone was adopted to stabilize the solution. The resulted solution was diluted to get a series of precursors, which was then spin coated onto Pt/Ti/SiO_2/Si substrates at a speed of 3,500 rps followed by a dry process at 400 °C for 4 min to remove organic compounds. After the above step repeated two times, the samples were normally crystallized at 750 °C (1 h in oxygen flow). X-ray diffractometer (XRD) equipped with Cu–Kα radiation was used to detect the crystalline structure of the samples, and Scanning probe microscope (SPM; Nano IV) was adopted to observe the surface morphology of them in the tapping mode. Each sample was scanned (512×512) in a region of 5×5 μm, while each scan was leveled before RMS, R_{max} were calculated. Here R_{max} is the maximum height over the scanned region minus the minimum height. Root mean square (RMS) is defined as below:

$$\mathrm{RMS} = \sqrt{\sum_{i=1}^{n}\sum_{j=1}^{m}\left(Z(i,j)-\overline{Z}\right)^2}\Big/ nm$$

3 Results and discussion

The effect of the Pt surface morphology versus annealing time was investigated. There are two kinds of grains on the annealed plane: the little mesas and relatively large hillocks. The mesas are primary on the Pt substrate and can grow larger in the annealing process. Notice that, after 10 min annealing, the formation of the thermal expansion mismatch caused Pt hillocks rise up the plane of the substrate, which lower the R_{max} and RMS values. For annealing time of 20 min, the growths of the Pt mesas become clearly coinstantaneous with the protuberances of the Pt substrates, which increase the R_{max} and RMS values. In the following annealing process from 20 min to 1 h, the protuberances of the Pt substrates make the Pt hillocks cover up the primal Pt mesas gradually. It reduces the RMS value of the surface. Of course all the changes discussed here are only in the region of several nanometers. After 1 h, height of the Pt hillocks increases dramatically and the R_{max} and RMS values increase continuously. In order to acquire ideal self-patterning $Bi_{3.25}Nd_{0.85}Ti_3O_{12}$ grains and decrease the effect of Pt substrate, all the annealing time in our experiments is thus set to be less than 60 min.

Figure 1 is a plot of surfaces for 0.001, 0.005, 0.008, 0.01, 0.02, and 0.05 mol/l BNT deposited on Pt(111)/Ti/SiO_2/Si substrate by MOD method. All the samples were baked at 400 °C for 4 min and annealed at 750 °C for 1 h in oxygen flow. The RMS and R_{max} values of these samples are shown in Fig. 2. Notice an abrupt increase of RMS at the precursors' concentration from 0.003 to 0.005 mol/l; with the further rising of concentration, a sharp decease

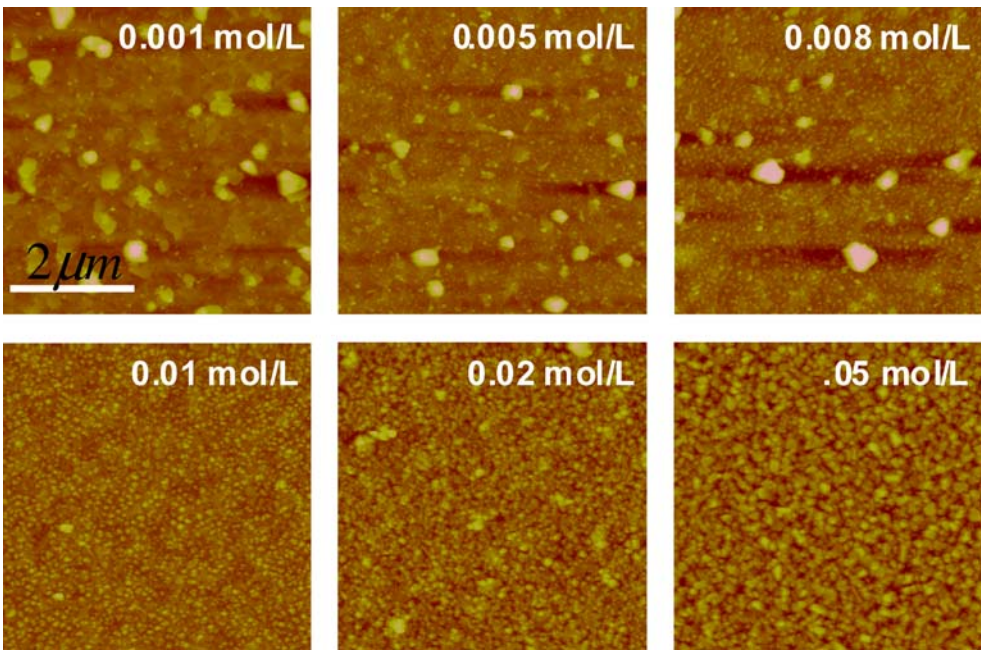

Fig. 1 Surface morphology of a series of $Bi_{3.15}Nd_{0.85}Ti_3O_{12}$ samples deposited on Pt/Ti/SiO_2/Si substrates 750 °C annealing

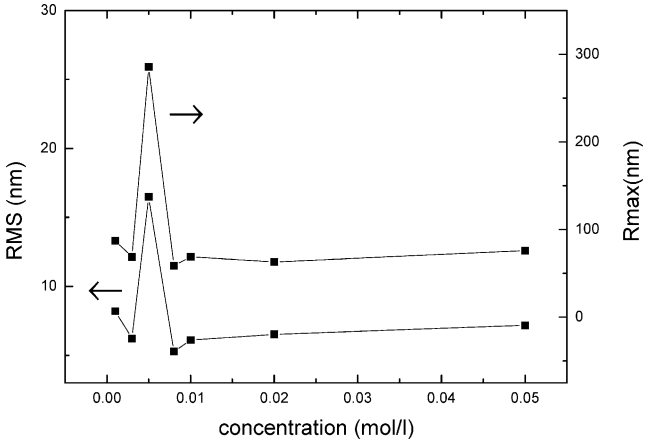

Fig. 2 RMS and R_{max} values versus precursors' concentration of $Bi_{3.15}Nd_{0.85}Ti_3O_{12}$ samples

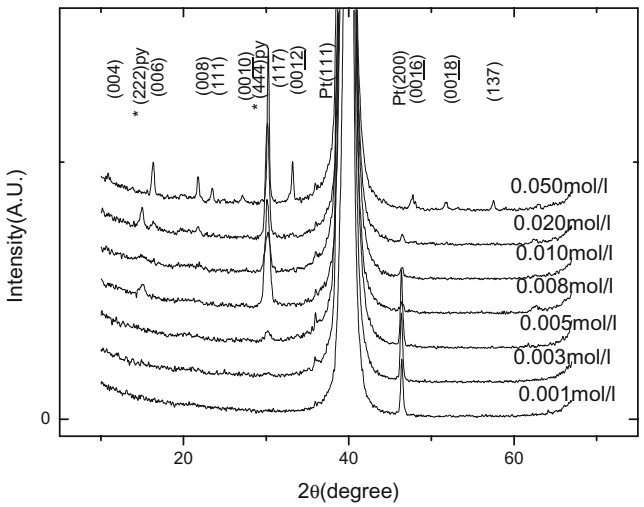

Fig. 4 XRD patterns of a series of $Bi_{3.15}Nd_{0.85}Ti_3O_{12}$ samples with different precursors' concentration, 10% Bi excess

occurs at nearly 0.008 mol/l. After that, the RMS values nearly have no change. The R_{max} value versus concentration reveals the same tendency as shown in the right plot of Fig. 2. We think that this kind of change can be attributed to two aspects: one, the variation of the surface morphology of the annealed Pt substrates; two, the nucleation and growth process of the BNT nanoparticles. The relatively large Pt hillocks would form after annealing and strongly affect the morphology of the Pt substrates with increasing annealing time [9]. As seen in Fig. 2, when the precursor's concentration is rather low, the morphology of the annealed Pt substrate strongly affects the distribution of the BNT particles on the surface. At low concentration from 0.003 to 0.005 mol/l, nucleation of BNT preferentially occurs around the Pt hillocks and then grows larger, the R_{max} and RMS values increase as shown in Fig. 2. Above 0.005 mol/l, the nucleation could occur on the whole plane, which lower the R_{max} and RMS values. Continuously increasing the precursor's concentration to 0.008 mol/l represents the change from separated particles to consecutive thin film, the R_{max} and RMS values keep decreasing and remain almost unchanged afterwards. This kind of change may come from the alteration of the surface energy in the very thin films. At the concentration below 0.008 mol/l, large separated particles could reduce the surface energy. When concentration rising, the consecutive small grains would decrease the surface energy comparing with the large separated particles, and the consecutive thin film is formed. Above that, increasing the precursors' concentration would make the thin films become more compact and the R_{max} and RMS values of the samples nearly have no change.

The well-separated BNT nanoparticles were self-assembly fabricated at the precursor's concentration of 0.008 mol/l as shown in Fig. 3. The left plot is the cross section view and the right one is the morphology of the sample. The cross section view reveals the typical grain size of 20–25 nm in height and 100–150 nm in width.

To ensure the ferroelectricity of the nanoscale memory units, the formation of the perovskite phase is important. In our experiment, XRD was adopted to characterize the crystalline structure of the BNT samples with different precursors' concentration and Bi excess. XRD patterns of this series of BNT samples are shown in Fig. 4. The samples with the precursors' concentration below 0.005 mol/l show nearly no diffraction peaks belong to the BNT perovskite structure for the rather low concentration. At the precursor's concentration of 0.005 mol/l the diffraction peak with 2θ near 30° appears. Magnifying the

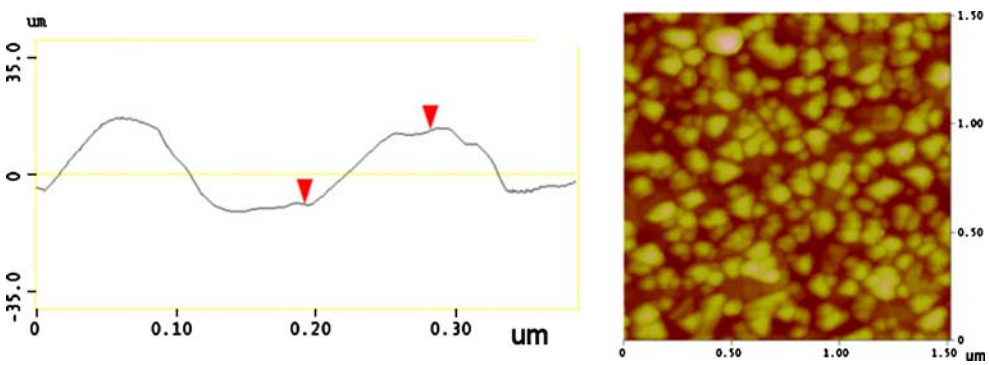

Fig. 3 The plain view and cross section view of the separated nanoparticles with the precursor's concentration of 0.008 mol/l

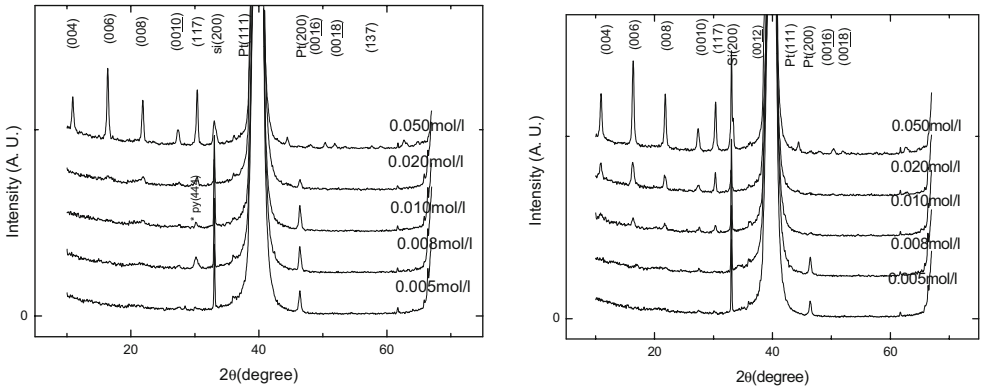

Fig. 5 (**a**) XRD patterns of a series of $Bi_{3.15}Nd_{0.85}Ti_3O_{12}$ samples with different precursors' concentration, 20% Bi excess (*left*). (**b**) 30% Bi excess (*right*)

peak and it can be seen to be a combination of the pyrochlore (444) diffraction plane and the perovskite (117) diffraction plane. Increasing the concentration to 0.008 mol/l, the peak mentioned above becomes more obvious and the pyrochlore (222) plane appears. The samples of 0.01 mol/l and 0.02 mol/l reveal some inconspicuous peaks belonging to the perovskite structure besides the pyrochlore (444), pyrochlore (222), and perovskite (117) peaks mentioned above. In the diffraction patterns of the 0.05 mol/l BNT, the pyrochlore phase disappear and the perovskite diffraction peaks are clear and pure. The emergence of the pyrochlore (444) and (222) peaks is caused by the high volatility of the Bi element in the separated nanoparticles. Comparing with the compact thin films, these separated particles have larger ratio of surface versus volume. In this case, 10% stoichiometric excess of Bi element is not sufficient for the volatile and the lack of Bi induced the emergence of the pyrochlore phase. Notice that the lower the precursors' concentration is, the more the particles are separated, and the more the pyrochlore phase ratio in all the diffraction patterns.

In order to reduce the ratio of pyrochlore phase, a series of BNT samples with 20, and 30% stoichiometric excess of Bi element were synthesized. The precursors' concentrations were 0.005, 0.008, 0.01, 0.02, and 0.05 mol/l. XRD patterns of these two series of samples are shown in Fig. 5(a) and (b). The two series of samples reveals the Si (200) diffraction peak, which disappears in the powder diffraction spectra. In the diffraction patterns of the 20% Bi excess samples, when the precursor's concentration is lower than 0.01 mol/l, pyrochlore (444) peak can be seen, while all the diffraction peaks in the 0.02 and 0.05 mol/l samples belong to the perovskite phase. For the 30% Bi excess series, the pyrochlore phase does not emerge at all, and all the diffraction patterns show pure perovskite phase. The above results give that: the more the Bi excess is, the lower the precursor's concentration is needed to form the pure perovskite phase nanoparticles. The 30% stoichiometric excess of Bi element is sufficient to compensate the volatile of Bi in the low concentration samples.

Piezoresponse detections are performed on the 0.008 mol/l sample, No obviously contrast owing to domains can be detected in the samples as shown in Fig. 6(a). Figure 6(b) gives the piezoresponse of the BNT consecutive film which was produced in the same conditions as the 0.008 mol/l samples, showing variation of domain structures among grains. We think that although the lateral sizes of the nano-grains are 100–150 nm, the height is only about 20 nm. So, the grains are probably in single domain state [10, 11].

4 Conclusion

Series of $Bi_{3.15}Nd_{0.85}Ti_3O_{12}$ samples were synthesized by MOD method. The morphology change of the Pt substrate versus annealing time is investigated to select an appropriate annealing time of 60 min. It seems that the change from separated BNT nanoparticles to consecutive thin film occurs at the precursor's concentration near 0.008 mol/l. Well separated particles were got with the precursor's

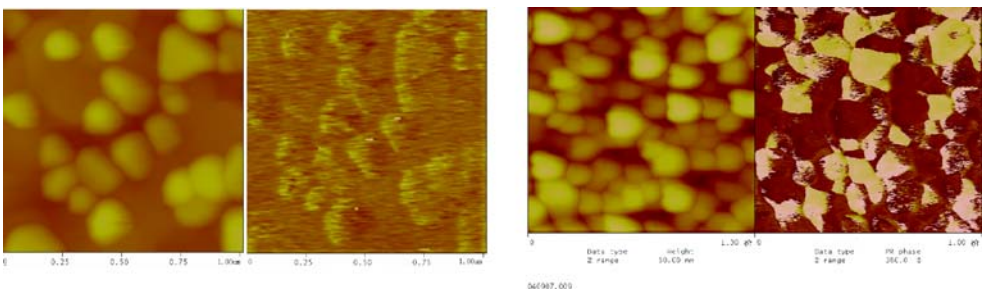

Fig. 6 (**a**) The single domain state of the BNT nanoparticles (*left*). Piezoresponse of the BNT thin films (*right*)

concentration at 0.008 mol/l. The typical size of these particles are 20–25 nm in height and 100–150 nm in width. XRD analysis reveals that the more the Bi excess is, the lower the precursor's concentration is needed to form the pure perovskite phase nanoparticles. This phenomenon can be attributed to the high volatile of Bi in the nanoparticles for their higher surface versus volume ratio comparing with the compact thin films. Piezoresponse detections show that the nanoparticles are mainly single domain structure. The appropriate conditions for the fabrication of Nd-substituted $Bi_4Ti_3O_{12}$ nanoparticles on $Pt/Ti/SiO_2/Si$ substrates might be: 30% Bi excess, 0.008 mol/l precursor's concentration, two coating, and 750 °C annealing.

Acknowledgment This work was supported by the National Science Foundation of China (No 90207027, 90401014), the 973 Project of MOST (2002CB613303) of China, and Jiangsu Natural Science Foundation (No. BK 2002410, BK2004084).

Reference

1. C.A. Paz de Araujo, J.D. Cuchiaro, L.D. McMillan, M.C. Scott, J. F. Scott, Nature (London). **374**, 627 (1995)
2. P.H. Park, B.S. Kang, S.D. Bu, T.W. Noh, J. Lee, W. Jo, Nature (London). **401**, 682 (1999)
3. T. Watanabe, T. Kojima, T. Sakai, H. Funakubo, M. Osada, Y. Noguchi, M. Miyayama, J. Appl. Phys. **92**, 1518 (2002)
4. T. Kojima, T. Sakai, T. Watanabe, H. Funakubo, Appl. Phys. Lett. **80**, 2746 (2002)
5. I. Szafraniak, C. Harnagea, R. Scholz, S. Bhattacharyya, D. Hesse, M. Alexe, Appl. Phys. Lett. **83**, 2211 (2003)
6. M. Alexe, J.F. Scott, C. Curran, N.D. Zakharov, D. Hesse, A. Pignolet, Appl. Phys. Lett. **73**, 1592 (1998)
7. J.F. Scott, M. Alexe, N.D. Zakharov, A. Pignolet, C. Curran, D. Hesse, Integr. Ferroelectr. **21**, 1 (1998)
8. S.K. Lee, W. Lee, M. Alexe, K. Nielsch, D. Hesse, U. Gosele, Appl. Phys. Lett. **86**, 152906 (2005)
9. S.R. Summerfelt, D. Kotecki, A. Kingon, H.N. Alshareef, Mat. Res. Coc. Symp. Proc. **361**, 257 (1995)
10. S.B. Ren, C.J. Lu, J.S. Liu, H.M. Shen, Y.N. Wang, Phys. Rev. B (Rap. Commun). **54**, R14337 (1996)
11. S.B. Ren, C.J. Lu, H.M. Shen, Y.N. Wang, Phys. Rev. B. **55**, 3485 (1997)